Tailoring Electron Diffusion in Electrospun Metal Oxide Nanostructures for Dye-sensitized Solar Cells

R. Jose,[*] P. S. Archana,[**] A. Le Viet,[**] E. Naveen Kumar,[**] M. M. Yusoff,[*] S. Ramakrishna[**]

[*]Faculty of Industrial Sciences and Technology, Universiti Malaysia Pahang, 26300 Kuantan, Malaysia.
rjose@ump.edu.my

[**]Nanoscience and Nanotechnology Initiative, National University of Singapore, 117576 Singapore

ABSTRACT

Metal oxide wide bandgap semiconducting nanostructures lie at the heart of many technologies including dye-sensitized solar cells (DSCs). In DSCs, they act as charge separation and transport medium; and therefore, understanding and controlling charge transport is key to increase the performance level of corresponding devices beyond current thresholds. Unlike bulk semiconductors, in which the electrons diffuses in the conduction band from one transport state to another, electron transport in nanostructured materials occurs through the localized surface energy states that lie within the bandgap. This article focus on the advances made on controlling the charge transport in electrospun metal oxide nanostructures.

Keywords: Dye-sensitized solar cells, Electron diffusion, Electrospinning, Metal oxide semiconductors

1 INTRODUCTION

Dye-sensitized solar cells (DSCs) have emerged as one of the low-cost photovoltaic device due to less fabrication cost and less-expensive raw materials. The photovoltaic effect in DSCs occurs at the interface between a dye-anchored wide bandgap nanostructured metal oxide semiconductor (n-MOS) and a redox electrolyte [1]. Intensity of solar light is weak at the absorption wavelength window of most MOSs, which is conventionally widened by sensitizing by organic flourophores (dyes), hence the name dye-sensitized solar cells. On sunlight irradiation, the dye absorbs solar light thereby creates a transiently localized state called exciton. The exciton can be viewed as a quasi particle composing an (e^-–h^+) pair. If the conduction band energy of the MOS is at lower energies than the lower unoccupied molecular orbital (LUMO) of the dye, then the excited electron decays to the MOS and thereby creating mobile charge carriers [2]. The electrons injected to the conduction band of the oxide material is transported through the mesoporous network to the counter electrode by doing a work equal to the energy difference between the conduction band of the electrode and redox potential of the electrolyte. The oxidized dye is regenerated by a hole-conductor, thereby completing the cycle of operations.

The photoconversion efficiency (η) of DSCs, from a first principle approach, depends on the amount of the dye used in the cell as they are the primary absorbers of solar light. Although the n-MOS absorb solar light, the intensity of the solar spectrum is rather weak at their bandgaps (~3.2 eV). Need for more amounts of dye demands more amounts of active metal oxide surface to bind them, which could be achieved by using mesoporous materials of large specific surface area and/or increasing the thickness of the n-MOS network. However, mesoporous materials are weakly crystalline that are disadvantageous for efficient charge transport. In addition, there are intrinsic limitations to increase the thickness of the electrode film because the photoinjected carriers recombine with the electrolyte if they take longer time to reach the anode than their lifetime. The time required for photoelectrons to reach the anode is known as the electron transit time and is a crucial parameter in DSCs. The electrons travels a distance equals to the electron diffusion length in electron transit time. The diffusion length is given by $L = (D_n \tau)^{1/2}$, where D_n is the electron diffusion coefficient and τ is the electron lifetime. The electron lifetime in DSCs is ~10^{-6} s, which limits the diffusion length to be several microns assuming the D_n to be 10^{-4} cm^2/s [2]. For efficient charge collection in DSCs, the thickness of the mesoporous metal oxide electrode should be one-third of the diffusion length. Therefore, development of materials with high D_n while maintaining large surface area and high crystallinity are most proming ways to increase the η of DSCs. Research over the past decade brought the η of DSCs to 12% [3]. The state-of-the art DSC uses a mesoporous TiO_2 particles sensitized by an organic sensitizer organic sensitizer Carbz-PAHTDTT and ferrocene-based electrolyte [3].

This paper describes advanced materials featured by high D_n. The materials were developed by electrospinning a polymeric solution and subsequent controlled annealing [4, 5]. This paper reports four materials characterized by high D_n, viz. one-dimensional (1D) anatase TiO_2, Nb doped TiO_2, Nb_2O_5 and SnO_2.

2 EXPERIMENTAL DETAILS

Samples for analysis were 1D nanostructures developed by electrospinning a polymeric solution and subsequent annealing [4, 5]. Four typical materials are presented here, their respective processing details could be found from the noted references. (1) TiO_2 nanofibers, nanowires, and nanorods [6-8] ; (2) Nb-doped TiO_2 nanofibers [9, 10]; (3) monoclinic Nb_2O_5 nanonuggets [11, 12]; (4) SnO_2 flowers [13].

2.1 Fabrication and Characterization of DSCs

The TiO_2 electrodes were prepared as described before [6-15]. The TiO_2 nanorod electrodes (area ~1 cm^2) were soaked in a 1:1 vol. mixture of acetonitrile and *tert*-butanol with ruthenium dye ($RuL_2(NCS)_2$-$2H_2O$; L=2.2'-bipyridyl-4,4'-dicarboxylic acid (0.5 mM, N3 Solaronix) for 12 h at room temperature. The soaked electrodes were washed with ethanol to remove non-anchored dye molecules and then dried in the air. Pt sputtered FTO glasses were used as counter electrode. The Pt counter electrode and the dye anchored TiO_2 electrode were assembled into a sealed sandwich type cell using a sealing material (SX1170-25, film thickness = 25 μm, Solaronix). Acetonitrile containing 0.1M lithium iodide, 0.03M iodine, 0.5M 4-*tert*-butylpyridine, and 0.6M 1-propyl-2,3-dimethyl imidazolium iodide was used as redox electrolyte solution. The electrolyte solution was injected into the cell through a small opening drilled on the counter electrode. Finally the opening was sealed by a piece of glass.

Current-voltage characteristics and electrochemical impedance spectroscopy (EIS) data were obtained using a potentiostat (Autolab PGSTAT30, Eco Chemie B.V., The Netherlands). The EIS measurements were carried out in the dark using 10 mV ac voltage superimposed on a forward-biased DSC (0.4–0.7 V) with frequency ranging from 30 kHz to 0.05 Hz. The electron transport were also studied using transient photocurrent technique, the details of which are available in our earlier publications [8, 9].

3 RESULTS AND DISCUSSION

3.1 Charge transport Mechanism in n-MOS

Electron transport through metal oxide nanostructures has been fairly well understood. In bulk single crystalline n-MOS, electrons in the conduction band move from one transport state to another with a free electron diffusion coefficient (D_O) of ~10^{-1} cm^2/s. The extended periodicity in the bulk crystal is altered in amorphous and nanocrystalline semiconductors, and thereby, alter their electronic band structure and eventually the free electron diffusion mechanism become less dominant. In n-MOS, electrons move via extended band-tail states at the bottom of the conduction band as well as broad distribution of localized energy states lie within the bandgap [16]. Density of those localized states is higher at the bottom of the conduction band and exponentially decreases in the energy scale towards the top of the valence band (Fig.1). The carriers injected to the n-MOS are trapped by the band-tail states and subsequent thermal activation leads the electrons to deeper energy levels and retrap again (Fig. 1). The injected carriers thus move via a trap-detrap, otherwise called multiple trapping (MT), mechanism through the transport level (E_{TR}); the E_{TR} is a function of Fermi level [17]. In the case of DSCs, the photoinjected electrons increase the chemical capacitance (C_μ) of n-MOS [18] and the consequent D_n through E_{TR} typically is ~10^{-7}–10^{-5} cm^2/s for lower photoexcitation density ($\Phi \leq 10^{16}$ cm^{-3}) [19], typically for n-TiO_2. i.e., the D_n in n-TiO_2 is several orders of magnitude lower than D_O due to the above described trap-limited diffusion process. Kopidakis et al showed that higher Φ ($\geq 10^{17}$ cm^{-3}) uplift the Fermi level of n-TiO_2 close to its extended band-tail states and result in a diffusion mechanism similar but lower in magnitude (D_n ~10^{-4} cm^2/s) to that of the bulk TiO_2 [19].

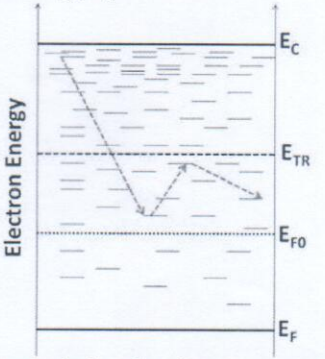

Figure 1: Cartoon depicting the charge transport process in nanostructured metal oxide semiconductors. The E_F and E_{F0} are the Fermi and psudo-Fermi energies, E_{TR} is the electron transport energy, and E_C is the conduction band energy.

3.2 Charge transport through 1-D TiO_2 Nanostructures

Table 1 shows the photovoltaic parameters of the various TiO_2 devices used in this study.

Table 1: Photovoltaic properties of the devices used for the current study. J_{SC} – Current density; V_{OC} – Open circuit voltage; FF – Fill Factor; η – Efficiency

Morphology	J_{SC} (mA/cm^2)	V_{OC} (V)	FF (%)	η (%)
TiO_2 Fibers [6]	9.45	0.78	57	4.2
TiO_2 rods [7]	13	0.83	49	5.2
TiO_2 wires [8]	8.46	0.82	60	4.3
Nb:TiO_2 [10]	14.79	0.72	57	6
TiO_2 NPs [21]	17.05	0.86	76	11

Figure 2 show sthe Nyquist plots of a representative nanofiber device recorded at under different bias in the dark. The high frequency offset is the series resistance *Rs* of the cell, primarily due to the FTO resistance. The platinum/electrolyte interface can be seen as the small arc at high frequencies. The transport and charge transfer processes in the Nb:TiO_2 nanofibers, prominent at low bias, show up as a straight line followed by the larger arc at intermediate frequencies, respectively. Diffusion in the electrolyte can be detected as a small arc at low frequencies.

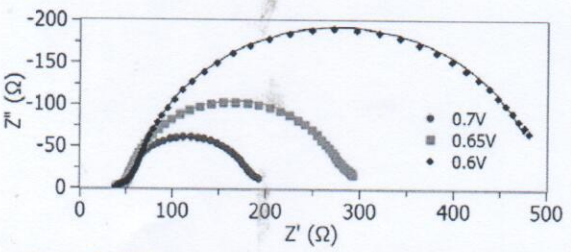

Figure 2: EIS spectra of nanofiber based devices

The EIS data was fitted to the well-accepted diffusion-recombination model, the resistors and capacitors in which represents various interfacial and transport processes in DSCs, to extract the effective electron diffusion coefficient in TiO_2, electron transit time, and lifetime [20, 21] Details of the transmission line model are as described elsewhere [21]. For a device of electrode thickness L, the electron transport resistance in the TiO_2 nanofiber is $R_T=r_tL$ is strongly dependant on the crystallinity of the material. The charge transfer resistance $R_{CT}=r_{ct}/L$ and $C_\mu=c_\mu/L$ are indicative of recombination with the electrolyte and electron density in Nb:TiO_2, respectively. The r_t, c_μ and r_{ct}, are components of the transmission line as defined in reference 21. The electron lifetime (τ_n) and transit time (τ_d) are given by $\tau_n=(r_{ct}c_\mu)^{1/\beta}$ and $\tau_d=\tau_n(R_T/R_{CT})^{1/\beta}$ where β is the CPE exponent. The effective diffusion coefficient is then computed as $D_n=L^2/\tau_d$ [21].

Figure 3 shows the variation of D_n of the TiO_2 devices. Performances of four devices are shown: (i) nanoparticle based device characterized by the highest efficiency; (ii) nanorod based device, and (iii) continuous nanofiber based device and (iv) Nb doped nanofiber based device. Among them nanorod based devices showed marked difference in the diffusion behavior compared to the rest, in which the D_n depended very weakly on the applied voltage. In all the other cells, the dependence of D_n on the applied voltage is appreciable. The strong dependence arise from the trap-detrap diffusion as explained before. Two regions were observed in the D_n vs. applied voltage graph of Nb:TiO_2 (i) 0.4 – 0.6 V region a region with two orders of magnitude enhanced D_n (~10^{-4} cm^2/s) compared to the undoped samples and with a weak dependence on applied voltage and (ii) >0.6 V region, where D_n (~10^{-3} cm^2/s) is independent of the applied voltage indicating the diffusion through the extended states. Enhanced D_n and weak dependence on applied voltage should arise from the larger C_μ of the Nb:TiO_2 achieved through doping. In contrast, for the *n*-TiO_2 based devices, the D_n depended strongly on the applied voltage, which was explained on the basis of trapping-detrapping model. The Fermi level increases with the applied voltage and removes some of the deep traps, and therefore, E_{TR} level shifts near to the extended band tail states and result in D_n ~10^{-4} cm^2/s, typically in *n*-TiO_2. The Nb:TiO_2 showed similar diffusion behavior even at lower bias voltages, which indicate that doping shifted the E_{TR} to the extended states. Further enhancement of the applied voltage above 0.6 V did not change the D_n and this quantity was two orders of magnitude lower than D_O. This difference would probably arise from the inferior crystallinity of Nb:TiO_2 nanofibers compared to the bulk crystals.

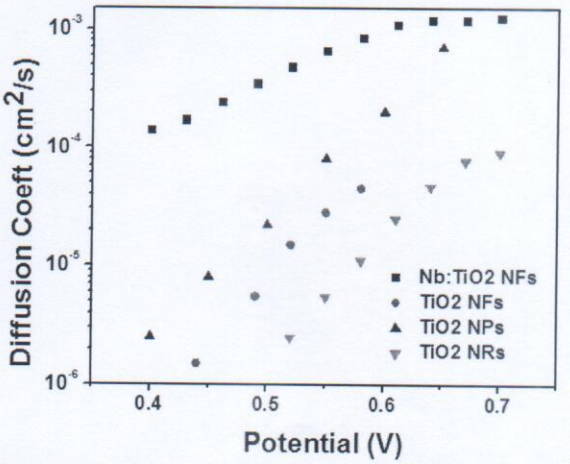

Figure 3: Electron diffusion coefficients of TiO_2 morphologies considered in this work

3.3 Charge transport through Nb_2O_5 and SnO_2 nanostructures

In addition to TiO_2, which have the advantages of getting mesoporous materials relatively easy, there are other wide bandgap metal oxides such as Nb_2O_5 and SnO_2. Both SnO_2 and Nb_2O_5 has defenite advantages over TiO_2: Nb_2O_5 has a higher conduction band edge compared to TiO_2 hence offer possibilities for higher V_{OC} and SnO_2 has higher electron mobility compared to TiO_2 hence possible to attain higher photovoltaic performances [2].

The Nb_2O_5 has several polymorphs: choice of proper polymorph has been recently addressed by us and identified that monoclinic Nb_2O_5 has desirable charge transport properties [11]. Samples for the present study were nano-nuggets. Due to high processing temperature involved, specific surface area of the of the materials used for device fabrication was rather poor and the efficiency of the corresponing device was ~2%. Figure 4 shows the electron lifetime and D_n of the DSCs fabricated using monoclinic Nb_2O_5. Both lifetime and D_n depend strongly on the applied

voltage thereby indicating trap limited diffusion behavior. The D_n of Nb_2O_5 based devices were comparable with that of Nb doped TiO_2.

The SnO_2 nanostructures with different morphologies such as fibers and flowers were synthesized, their details will be published elsewhere [13]. The differences in electrical properties of these two morphologies were determined EIS measurements of the DSCs in the dark under forward bias. The Nyquist plots (Data not shown) showed that radius of the right semicircle of the flower based device is larger compared to that made using the fibers. The apparently larger semicircle indicates increase in the charge transfer resistance; and therefore, an increased electron lifetime. The D_n determimed from the EIS spectra were ~10^{-3} cm^2/s at 0.7 V, which is comparable to that of the Nb doped TiO_2 and Nb_2O_5 nanonuggets.

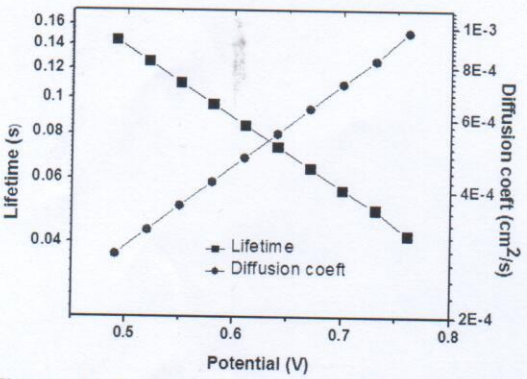

Figure 5: Electron diffusion coefficient of monoclinic Nb_2O_5

Finally, the charge mobility through the above nanostructures were studied by transient photocurrent measurements. The D_n derived from the EIS plots were in good agreement the transient photocurrent measurements. Table 2 summarizes the electron mobility values of the various nanostructures considered under present study. Among them Nb doped TiO_2 showed the highest electron mobility among them followed by SnO_2 flowers. The Nb doped TiO_2 could, therefore, soon find electronic applications requiring high electron mobility and optical transparency

Table 2: Electron Mobilities of the samples used in this study

Morphology	Normalized Transit time [ms]	Normalized Electron Mobility [$cm^2 V^{-1}s^{-1}$] x 10^{-3}
SnO_2 Fibers	10	3.75
SnO_2 Flowers	2	18.5
Nb: TiO_2	0.2	185
TiO_2 Nanowires	5.5	6.74
TiO_2 NPs	15	2.47

ACKNOWLEDGEMENTS

This work was in part financially supported by the Universiti Malaysia Pahang (RDU10337)

REFERENCES

[1] M. Grätzel, Inorg. Chem. 44, 6841 (2005).
[2] R. Jose, V. Thavasi, S. Ramakrishna, J. Am. Ceram. Soc.92, 289 (2009).
[3] T. Daeneke, T. H. Kwon, A. B. Holmes, N. W. Duffy, U. Bach, L. Spiccia, Nature Chem. 3, 211 (2011).
[4] S. Ramakrishna, R. Jose, P. S. Archana, A. S. Nair, R. Balamurugan, J. R. Venugopal, W. E. Teo, J. Mater. Sci. 45, 6283 (2010).
[5] R. Ramasheshan, S. Sundarrajan, R. Jose, S. Ramakrishna, J. Appl. Phys.102, 111101 (2007).
[6] K. Mukherjee, T. H. Teng, R. Jose, S. Ramakrishna, Appl. Phys. Lett. 95, 012101 (2009).
[7] K. Fujihara, A. Kumar, R. Jose, S. Ramakrishna, S. Uchida, Nanotechnology 18, 365709 (2007).
[8] P. S. Archana, R. Jose, C. Vijila, S. Ramakrishna, J. Phys. Chem. C 113, 21538 (2009).
[9] P. S. Archana, R. Jose, T. M. Jin, C. Vijila, M. M. Yusoff, S. Ramakrishna, J. Am. Ceram. Soc. 93, 4096 (2009).
[10] P. S. Archana, R. Jose, M. M. Yusoff, S. Ramakrishna, App. Phys. Lett. 98, 152106 (2011).
[11] A. Le Viet, R. Jose, M. V. Reddy, B. V. R. Chowdari, S. Ramakrishna, J. Phys. Chem. C 114, 21795 (2010).
[12] A. Le Viet, M. V. Reddy, R. Jose, B. V. R. Chowdari, S. Ramakrishna, J. Phys. Chem. C 114, 664 (2010).
[13] E. Naveen Kumar, R. Jose, P. S. Archana, A. S. Nair, C. Vijila, S. Ramakrishna, Submitted (2011).
[14] R. Jose, A. Kumar, V. Thavasi, S. Ramakrishna, Nanotechnology 19, 424004 (2008).
[15] R. Jose, A. Kumar, V. Thavasi, K. Fujihara, S. Uchida, S. Ramakrishna, Appl. Phys. Lett. 93, 023125 (2008).
[16] D. Monroe, Phys. Rev. Lett. 54, 146-149 (1985).
[17] J. Bisquert, J. Phys. Chem. C 111, 17163 (2007).
[18] J. Bisquert, Phys. Chem. Chem. Phys. 5, 5360 (2003).
[19] N. Kopidakis, K. D. Benkstein, J. van de Lagemaat, A. J. Frank, Q. Yuan, E. A. Schiff, Phys. Rev.B 73, 045326 (2006).
[20] J. Bisquert, G. Garcia-Belmonte, F. Fabregat-Santiago, N. S. Ferriols, P. Bogdanoff, E. C. Pereira, J. Phys. Chem. B 104, 2287 (2000).
[21] Q. Wang, S. Ito, M. Grätzel, F. Fabregat-Santiago, I. Mora-Sero, J. Bisquert, T. Bessho, H. Imai, J. Phys. Chem. B 110, 25210 (2006).